Research paper

Struct Multidisc Optim 27, 1–19 (2004)
DOI 10.1007/s00158-003-0363-y

Structural shape and topology optimization in a level-set-based framework of region representation

X. Wang, M.Y. Wang and D. Guo

Abstract In this paper we present a new framework to approach the problem of structural shape and topology optimization. We use a level-set method as a region representation with a moving boundary model. As a boundary optimization problem, the structural boundary description is implicitly embedded in a scalar function as its "iso-surfaces." Such level-set models are flexible in handling complex topological changes and are concise in describing the material regions of the structure. Furthermore, by using a simple Hamilton–Jacobi convection equation, the movement of the implicit moving boundaries of the structure is driven by a transformation of the objective and the constraints into a speed function that defines the level-set propagation. The result is a 3D structural optimization technique that demonstrates outstanding flexibility in handling topological changes, the fidelity of boundary representation, and the degree of automation, comparing favorably with other methods in the literature based on explicit boundary variation or homogenization. We present two numerical techniques of conjugate mapping and variational regularization for further enhancement of the level-set computation, in addition to the use of efficient up-wind schemes. The method is tested with several examples of a linear elastic structure that are widely reported in the topology optimization literature.

Key words structural optimization, topology optimization, shape optimization, boundary optimization, level-set methods, region representation

Received: 2 August 2002
Revised manuscript received: 26 June 2003
Published online: 1 April 2004

X. Wang[1], M.Y. Wang[2,✉] and D. Guo[1]

[1] School of Mechanical Engineering, Dalian University of Technology, Dalian 116024, China
[2] Department of Automation & Computer-Aided Engineering, The Chinese University of Hong Kong, Shatin, NT, Hong Kong
e-mail: yuwang@acae.cuhk.edu.hk

1 Introduction

In this paper we address the problem of shape and topology optimization of a linearly elastic structure to meet a design objective and to satisfy certain constraints. The problem is formulated in a level-set framework in which the design domain is described by a structural boundary that is embedded in a scalar function of higher dimensionality. As a *level set* or an *"iso-contour"* of the embedding function (also called the *level-set function*), the boundary is implicitly described without the need of an explicit representation. The optimization process is captured by a Hamilton–Jacobi-type partial differential equation (PDE) that governs the dynamic movement of the embedding function and hence changes in the structural boundary in accordance with the design objective and the constraints. While the shape and connectivity (i.e., topology) of the boundary may undergo drastic changes, the level-set function remains simple in its topology. Therefore, by a direct and efficient computation in the embedding space, the design boundaries can be tracked to a required level of accuracy, yielding an optimal structure in both shape and topology. The level-set models are referred to as a *region representation* and they can easily represent complex boundaries that can form holes, split into multiple pieces, or merge with others to form a single one. Based on the concept of propagation of the level-set interface, an optimization algorithm is derived from the shape sensitivity and the variations of the level-set embedded boundary.

Boundary-based shape optimization has been a major method for structural design (Rozvany 1989; Sokolowski 1992). In essence, the design domain is directly represented by its boundary, and a set of design variables directly controls the exterior and interior boundary shapes, for example, through the control points of B-splines. Based on a boundary shape sensitivity analysis, necessary boundary variations for the optimality conditions would provide the foundation of an optimization technique (Sokolowski 1992). It is a direct approach and it

is concise in the sense that the geometric boundary of the structure is expressed explicitly. Therefore, it generally allows more explicit representation of any features to be incorporated in the design. A major limitation of an explicit boundary representation, however, is that the connectivity of the boundary, or the topology of the structure, is *fixed*. A *conventional* boundary-based approach is not capable of handling topological changes for structural optimization (Bendsoe 1977; Rozvany 1988).

Perhaps with the major motivation of overcoming the fixed-topology limitation, various other techniques and approaches have been developed during the past decade. As the state-of-the-art, homogenization-based methods have become the main approach to structural optimization (Allaire 1997; Bendsoe 1988, 1989, 1993, 1997, 1999), in which a material model with micro-scale voids is introduced and the topology optimization problem is defined by seeking the optimal porosity of such a porous medium using one of the optimality criteria. By transforming the difficult topology design problem into a relatively easier "sizing" problem, the homogenization technique is capable of producing internal holes without prior knowledge of their existence. That is, it offers a tool for simultaneous shape and topology optimization. A number of variations of the homogenization method have been investigated to deal with these issues by penalizing intermediate densities, the "solid isotropic material with penalization" (SIMP) approach, in particular, for its conceptual and practical simplicity (Bendsoe 1989; Rozvany and Zhou 1991; Rozvany *et al.* 1992; Mlejnek 1992; Rozvany 2001). Material properties are assumed constant within each element used to discretize the design domain and the design variables are the element densities. The material properties are modeled to be proportional to the relative material density raised to some power. The power-law-based approach to topology optimization has been widely applied to problems with multiple constraints, multiple physics, and multiple materials (Bendsoe 1997; Bulman 2001; Diaz 1992; Rozvany 2001; Sigmund 2000, 2001; Suzuki 1991).

However, the homogenization method may not yield the intended results for some objectives in the mathematical modeling of structural design. It often produces designs with infinitesimal pores in the materials that make the structure not feasible. Further, numerical instabilities may introduce "non-physical" artifacts in the results and make the designs sensitive to variations in the loading (Bendsoe 1997; Bulman 2001; Rozvany 2001). Numerical instability and computational complexity remain major difficulties and are encountered in every realistic application. In our view, the root of these problems may well be related to the very reason for its success in other respects: its elimination of the boundary description. By treating the optimization problem as a material distribution problem, the homogenization-based approach (or the SIMP method) has fundamentally changed the nature of the problem. While there exist no geometric boundaries in the problem domain, there is no boundary connectivity to deal with; thus, there are no topological changes in a fundamental sense. In the end, the designer must interpret the resulting material distribution and extract a boundary and topological description, which is essential for obvious reasons (Lin 2000). These fundamental issues are still argued in the literature (Bendsoe 1999; Rozvany 2001).

Another class of approaches is essentially based on an evolutionary strategy called "evolutionary structural optimization" (ESO), which focuses on local consequences but not on the global optimum. It is typically computationally expensive since it has to rely on a "greedy-type" algorithm. A simple method of this class of optimization has been proposed by Xie and Steven (Xie 1997), which is based on the concept of gradually removing material to achieve an optimal design. The method was developed for various problems of structural optimization including stress considerations, frequency optimization, and stiffness constraints. A similar approach called "reverse adaptivity" was proposed by Reynolds *et al.* (1999), in which a fixed percentage of relatively under-stressed material is removed to find approximately fully stressed structures. Essentially, both evolutionary structural optimization and reverse adaptivity are homotopy methods based on so-called material "hard kills". In reverse adaptivity, finite element meshes near the boundary during the design procedure are refined to reduce computational costs or increase resolution.

Another approach is called the "bubble method", proposed by Eschenauer and Schumacher (Eschenauer 1994; Eschenauer 1997). In the method, so-called characteristic functions of the stresses, strains, and displacements are employed to determine the placement or insertion of holes of known shape at optimal positions in the structure, thus modifying the structural topology in a prescribed fashion. In this case, the design for a given topology is settled before its further changes.

Adopting the same principle of redesigning the structure based on the stress distribution in the current design, another approach was developed by Sethian and Wiegmann (2000) with a focus on the resolution of the boundaries. The boundaries are allowed to move according to the stresses on the boundaries. A level-set method is employed for tracking the motion of the structural boundaries under a speed function and in the presence of potential topological changes. An explicit jump immersed interface method is used for computing the solution of the elliptic problem in complex geometries without using meshes. The approach is also an evolutionary one. The principal idea is to remove material in regions of low stress and to add material in regions of high stress. A removal rate is established representing a percentage of the maximal initial stress below which material may be eliminated, and above which material should be added. The removal rate determines the closed stress contours along which new holes are cut and also the velocity of the boundary motion. The biggest benefit of this approach is that it is easier to add material (with some sub-grid

resolution) at hole boundaries with high stress than on a triangulated finite-element mesh. This approach seeks to improve design by making more efficient use of the material.

In our point of view, a boundary-based method with the capability of handling topology changes has the most promising potential. Boundary representations are always essential for design descriptions and for design automation with CAD and CAE systems. A major contribution of our work presented in this paper is the capability to capture topological changes with a region representation based on level-set methods. In our approach presented here, the structural boundaries are viewed as moving during the optimization process – interior boundaries (or holes) may merge with each other or with the exterior boundary and new holes may be created. The shape and topology optimization is carried out as a moving front of the level sets driven by the dynamics of the interior region under optimization conditions.

2 The optimization problem

In this paper we use a linear elastic structure to describe the problem of structural optimization. Conceptually, the approach presented here would apply to a general structure model. Let $\Omega \subseteq \mathrm{R}^n$ $(n = 2 \text{ or } 3)$ be an open and bounded set occupied by a linear isotropic elastic structure. The boundary of Ω consists of three parts: $\Gamma = \partial\Omega = \Gamma_d \cup \Gamma_u \cup \Gamma_t$, with Dirichlet boundary conditions on Γ_u and Neumann boundary conditions on Γ_t. It is assumed that Γ_d is traction free. The displacement field in Ω is the unique solution of the linear elastic system

$$
\begin{aligned}
&-\operatorname{div}\sigma(u) = p \quad \text{in } \Omega\,,\\
&u = u_0 \quad \text{on } \Gamma_u\,,\\
&\sigma(u)N = \tau \quad \text{on } \Gamma_t\,,
\end{aligned}
\tag{1}
$$

where the strain tensor ε and the stress tensor σ at any point $x \in \Omega$ are given in the usual form as

$$
\begin{aligned}
&\sigma_{ij}(u) = E_{ijkl}\varepsilon_{kl}(u)\,,\\
&\varepsilon_{ij}(u) = \frac{1}{2}\left(\frac{\partial u_i}{\partial x_j} + \frac{\partial u_j}{\partial x_i}\right)\,,
\end{aligned}
\tag{2}
$$

with E_{ijkl} the elasticity tensor, u_0 the prescribed displacement on Γ_u, τ the boundary traction force applied on Γ_t, p representing the applied body forces, and N the outward normal to the boundary.

The general problem of structure optimization is specified as

$$
\begin{aligned}
&\underset{\Omega}{\text{Minimize}} \quad J(u) = \int_{\Omega} F(u)\,\mathrm{d}\Omega\\
&\text{subject to}\\
&\int_{\Omega} E_{ijkl}\varepsilon_{ij}(u)\varepsilon_{kl}(v)\,\mathrm{d}\Omega = \\
&\int_{\Omega} pv\,\mathrm{d}\Omega + \int_{\Gamma_t} \tau v\,\mathrm{d}\Gamma, \quad \text{for all } v \in U\,,\\
&u = u_0 \quad \text{on } \Gamma_u\,,\\
&\int_{\Omega} \mathrm{d}\Omega \le V_{\max}\,.
\end{aligned}
\tag{3}
$$

Here, the linear elastic equilibrium equation is written in a weak variation form, with U denoting the space of kinematically admissible displacement fields. The inequality describes the limit on the amount of material in terms of the maximum admissible volume $V_{\max}$ of the design domain. The goal of structural optimization is to minimize the objective function $J(u)$ for a specific physical or geometric type described by $F(u)$. This is a standard notion of structural optimization (Bendsoe 1997; Sokolowski 1992).

3 Region models via level sets

Shape optimization is a general approach to the problem at hand. It is based on an analysis of shape sensitivity in terms of variations of the structural boundary. Standard procedures are well documented in the literature for obtaining the set of necessary conditions to be satisfied by an optimal solution (see, for example, Sokolowski 1992). A key concept in such an analysis is the "speed function" V_N of the optimality condition associated with a small variation in the boundary shape in the normal direction N. In general, it is necessary that

$$
V_N(x) = 0 \tag{4}
$$

everywhere on the design boundary Γ_d of the optimal structure. Physically, this indicates that the mutual energy form of the elastic structure reaches a constant value on Γ_d (Sokolowski 1992). In most shape optimization applications, directly solving this optimality equation is not possible. One general technique of shape optimization is to solve the ordinary differential equation

$$
\frac{\mathrm{d}x}{\mathrm{d}t} = V_N(x) \tag{5}
$$

with given initial boundary shape. The auxiliary variable t is denoted as the time-marching parameter. This is also known as the Lagrangian formulation of boundary propagation. When the steady state of this equation is achieved (i.e., $\mathrm{d}x/\mathrm{d}t = 0$), the optimality condition is also achieved and, hence, an optimal shape of the structure is obtained. This is the well-known *gradient descent* method

and there exist a large number of algorithms (Rozvany 1988; Sokolowski 1992).

In this conventional boundary-based method, the moving boundary is usually discretized with a set of design variables directly controlling the exterior and interior boundaries. The discrete design variables can be computed iteratively with an optimization algorithm and a finite element analysis. This often requires the construction of a new discrete model of the structure, or re-meshing, after each iteration. These issues have been extensively studied and there are well-established numerical methods and software systems for boundary shape design of structures (Sokolowski 1992). However, all of these methods utilize an explicit boundary representation and the boundary changes can be accomplished only if the connectivity of the boundaries does not change. In other words, they all have a severe limitation that only a structure of *fixed* topology can be optimized. For this reason, a boundary-based optimization has often been referred to as *shape optimization*. Topology changes in a structure mean that a boundary can "split" into pieces to form multiple boundaries or "holes". Conversely, several distinct boundaries may merge to make a single boundary. These changes provide the greatest challenge in a boundary-based approach to structural optimization.

As opposed to tracking the structural boundary with the Lagrangian formulation of (5), we suggest using an implicit function $\Phi(x)$ both to represent the boundary and to optimize it, as was originally developed for curve and surface evolution (Osher 1988; Sethian 1999). The change of the implicit function $\Phi(x)$ is governed by the simple convection equation

$$\frac{\partial \Phi(x,t)}{\partial t} + \nabla \Phi(x,t) \cdot V(x) = 0\,, \tag{6}$$

where $V(x)$ defines the "velocity" of each point on the boundary. This is also known as the Eulerian formulation of the boundary propagation, since the boundary is captured by the implicit function $\Phi(x)$ here. The velocity field $V(x)$ comes from an important concept of embedding the structural surface boundary as an iso-surface of the implicit function, $\Phi : R^n \mapsto R$, such that

$$\Gamma = \{x : \Phi(x) = k\}\ , \tag{7}$$

where k is the iso-value and is arbitrary, and x is a point in space on Φ. In other words, x is the set of points in R^n that composes the k-th iso-surface of Φ. The embedding Φ of $(n+1)$ dimensions can be specified in any specific form, for example, as a regular sampling on a rectilinear grid. A process of structural optimization can be described by letting the level-set function dynamically change in time. Thus, the dynamic model is expressed as

$$\Gamma(t) = \{x(t) : \Phi\left(x(t), t\right) = k\}\ . \tag{8}$$

By differentiating both sides of (8) with respect to time and applying the chain rule, we obtain the so-called Hamilton–Jacobi equation

$$\frac{\partial \Phi(x,t)}{\partial t} + \nabla \Phi(x,t) \frac{\mathrm{d}x}{\mathrm{d}t} = 0\,. \tag{9}$$

This equation defines an initial-value problem for the time-dependent function Φ. In this level-set model, $\mathrm{d}x/\mathrm{d}t$ is the velocity vector for shape optimization, $\mathrm{d}x/\mathrm{d}t = V(x)$. Thus, the optimal boundary is expressed as the solution of the partial differential equation on Φ:

$$\frac{\partial \Phi(x)}{\partial t} = -\nabla \Phi(x) \frac{\mathrm{d}x}{\mathrm{d}t} \equiv -\nabla \Phi(x) \cdot V(x)\,. \tag{10}$$

Furthermore, the local sign of $\Phi(x)$ can be used to define the inside and outside regions of the boundary such that

$$\begin{aligned} \Phi(x) &> 0 \quad \forall x \in \Omega \backslash \partial\Omega\,, \\ \Phi(x) &= 0 \quad \forall x \in \partial\Omega\,, \\ \Phi(x) &< 0 \quad \forall x \in \overline{\Omega} \backslash \Omega\,. \end{aligned} \tag{11}$$

The local unit normal to the surface N is given as

$$N = -\frac{\nabla \Phi}{|\nabla \Phi|} \quad \left(\text{where } |\nabla \Phi| = \sqrt{\nabla \Phi \cdot \nabla \Phi}\right)\,. \tag{12}$$

Since the tangential components of V vanish in (10), it can be written as

$$\frac{\partial \Phi(x)}{\partial t} = V_N \left|\nabla \Phi(x)\right|\ . \tag{13}$$

This is known as the *level set equation* (Osher 1988; Sethian 1999). As in (5), the normal velocity V_N is related to the sensitivity of the shape to the boundary variation and depends the objective of the optimization.

This formulation with level-set models has two major theoretical and practical advantages over conventional explicit boundary models, especially in the context of topology optimization. First, level-set models are topologically flexible. The scalar function Φ is defined to always have a simple topology; complicated surface shapes are implicitly represented by the level sets of Φ. The boundary shape representation is as general as the underlying physical theory. More importantly, the representation does not rely on any kind of explicit parameterization, along with no direct specification of the topology of the structure. These capabilities would allow the boundary models to easily change the structural topology while undergoing optimization in that they can form holes, split to form multiple boundaries, or merge with other boundaries to form a single surface. There is no need to re-parameterize the model as it undergoes significant changes in shape, in contrast to conventional boundary shape design (Sethian 1999). Further, the models can incorporate a large number of degrees of freedom and a number of numerical techniques have been developed (Osher 1988; Osher 2001; Sethian 1999) to make the initial value problem of (12) computationally robust and efficient. In fact, in the general case of a three-dimensional solid structure, the computational complexity can be

made proportional to the surface area of the structure rather than the size of its volume. We shall describe the details of the numerical computation of our proposed approach in the later sections.

Within this region model framework, our original problem of structural optimization (3) is described in terms of the level-set model as follows. We define a larger, fixed reference domain $\overline{\Omega}$ such that it fully contains the structure being optimized, Ω, i.e., $\Omega \subseteq \overline{\Omega}$. As described in (8), the boundary surface $\partial\Omega$ is implicitly defined as an iso-surface of the embedding $\Phi(x)$ such that $\Gamma = \{x : x \in \overline{\Omega},\ \Phi(x) = 0\}$. Here we use the convention that $k = 0$. The inside and outside regions of the geometric model are shown in Fig. 1 for a two-dimensional structure. In this case, the boundary curves are embedded in the three-dimensional function $\Phi(x)$ with a fixed topology. The surface of the embedding function may move up and down on a fixed coordinate system without ever altering its topology. The structural boundary curves embedded on $\Phi(x)$ can undergo drastic topological changes. However, there is no need to directly track these structural topological changes. The boundary optimization is implemented with the motion of $\Phi(x)$, and the topological changes in the boundary are discovered when the corresponding level set is computed.

With the level-set models, we can describe the optimal design problem in terms of the scalar function Φ. It is more convenient to use the Heaviside function H and the Dirac delta function δ, defined as

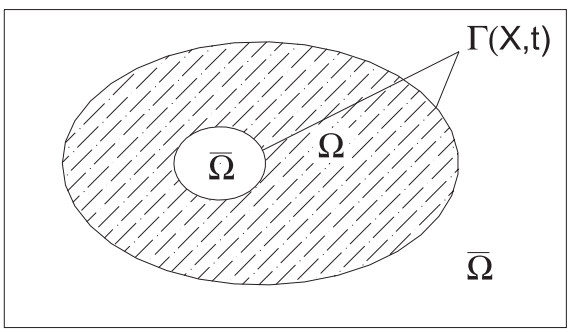

(a) The design domain Ω and its embedding domain $\overline{\Omega}$.

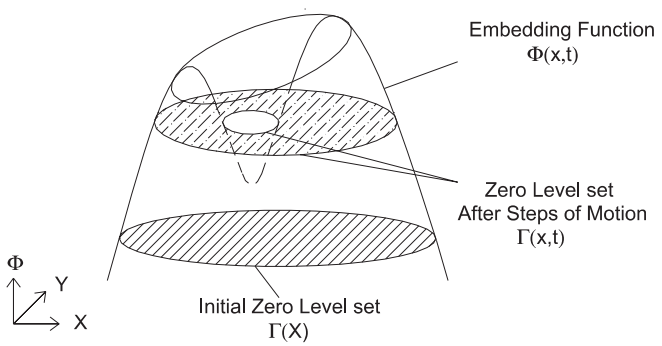

(b) The embedding function $\Phi(x)$ and the level set model Γ.

Fig. 1 The design domains and the boundary embedding with a level-set model

$$H(\Phi) = \begin{cases} 1 & \text{if } \Phi \geq 0 \\ 0 & \text{if } \Phi < 0 \end{cases} \quad \text{and} \quad \delta(\Phi) = \frac{\mathrm{d}H}{\mathrm{d}\Phi}\,. \tag{14}$$

Therefore, the optimization problem is now written as follows:

$$\underset{\Phi}{\text{Minimize}} \qquad J(u,\Phi) = \int_{\overline{\Omega}} F(u)H(\Phi)\,\mathrm{d}\Omega$$

subject to

$$a(u,v,\Phi) = L(v,\Phi) \quad \text{for all } v \in U\,,$$

$$u = u_0 \quad \text{on } \Gamma_{\mathrm{u}}\,,$$

$$V(\Phi) = \int_{\overline{\Omega}} H(\Phi)\,\mathrm{d}\Omega \leq V_{\max}\,, \tag{15}$$

where

$$a(u,v,\Phi) = \int_{\overline{\Omega}} E_{ijkl}\varepsilon_{ij}(u)\varepsilon_{kl}(v)H(\Phi)\,\mathrm{d}\Omega\,,$$

$$L(v,\Phi) = \int_{\overline{\Omega}} pvH(\Phi)\,\mathrm{d}\Omega + \int_{\overline{\Omega}} \tau v\delta(\Phi)\,|\nabla\Phi|\,\mathrm{d}\Omega \tag{16}$$

are the energy bilinear form and the load linear form respectively, and $V(\Phi)$ defines the volume of the structure.

4
Shape sensitivity and optimality conditions

With the formulation of (15), we are now ready to derive the necessary optimality conditions for the construction of an optimization procedure. The principal guideline for the optimization process is to move the design boundary represented by the level-set model according to its shape sensitivity with respect of the motion of the embedding function Φ, as shown in Fig. 1b. The key development of our application of the level-set methods here is to find an appropriate "speed function" V_N in (13) such that it will drive the design boundary into the optimum shape based on the given objective function and the constraint. The speed function must be expressed in terms of the level-set function Φ and must be linked to the derivative of the objective function with respect to the level-set variation. A highlight of our approach presented here is to bridge the well-established methods of shape sensitivity analysis (Sokolowski 1992) with the powerful methods of level sets (Osher 1988; Sethian 1999) to fulfill our goal of general structural optimization within the implicit boundary framework.

Using the standard Lagrangian multiplier method, we construct another objective function $\bar{J}(u,\Phi)$ and obtain a completely equivalent problem to the original optimization problem (15) as follows:

$$\underset{\Phi}{\text{Minimize}} \quad J(u,\Phi) = J(u,\Phi) + \lambda_+ \cdot (V(\Phi) - V_{\max})$$

subject to

$$a(u,v,\Phi) = L(v,\Phi)\,,\ u|_{\partial D_u} = u_0 \quad \text{for all } v \in U\,,$$

$$\lambda_+ \cdot (V(\Phi) - V_{\max}) = 0\,,$$

$$\lambda_+ \geq 0\,. \tag{17}$$

Here, λ_+ is the Lagrange multiplier and the last two constraints define a complementarity condition: When the inequality $V(\Phi) < V_{\max}$ is true, then $\lambda_+ = 0$; otherwise, when $V(\Phi) = V_{\max}$, $\lambda_+ > 0$. In order to derive the shape sensitivity, we follow the well-known approach of Murat and Simon (see, e.g., Allaire 2002; Sokolowski 1992). Thus, we define a perturbation of the optimal domain Ω^0 as

$$\Omega = (I + \psi)\,\Omega^0\,, \tag{18}$$

with ψ representing the perturbation vector field. The shape derivative of $\bar{J}(u,\Phi)$ at Ω^0 is then defined as the Fréchet derivative. This is a well-defined notion and it is derived in full detail in (Wang *et al.* 2003), with

$$\left\langle \frac{d\bar{J}(u,\Phi)}{d\Phi}, \psi \right\rangle = \int_{\overline{\Omega}} \delta(\Phi)\,(\beta\,(u,w,\Phi) + \lambda_+)\psi\,\mathrm{d}\Omega\ +$$

$$\int_{\partial\overline{\Omega}} \frac{\delta(\Phi)}{|\nabla\Phi|}\frac{\partial\Phi}{\partial N}\psi\,\mathrm{d}\Gamma\,, \tag{19}$$

where w represents the adjoint displacement in the conjugate equation

$$a(v,w,\Phi) = \langle J_u(u,\Phi), v\rangle \equiv \int_{\overline{\Omega}} \frac{\partial F(u)}{\partial u} v H(\Phi)\,\mathrm{d}\Omega\,,$$

$$w|_{\partial\Gamma_u} = 0 \quad \forall v \in U\,, \tag{20}$$

and

$$\beta(u,w,\Phi) = F(u) + pw - \tau w\kappa - E_{ijkl}\varepsilon_{ij}(u)\varepsilon_{kl}(w)\,, \tag{21}$$

with $\kappa = \nabla\cdot(\nabla\Phi/|\nabla\Phi|)$ being the mean curvature of the level-set surface. Thus, the Kuhn–Tucker condition of the optimal solution becomes

$$\beta(u,w,\Phi) + \lambda_+|_{\partial\Omega} = 0\,,$$

$$\lambda_+ \cdot (V(\Phi) - V_{\max}) = 0\,,$$

$$\lambda_+ \geq 0\,. \tag{22}$$

We can then construct the speed function $V_N(x)$ from the following equations:

$$V_N(x) = -\beta\,(u,w,\Phi) - \lambda_+\,,$$

$$\lambda_+ = -\int_{\partial\overline{\Omega}} \beta\,(u,w,\Phi)\ \mathrm{d}\Gamma \Big/ \int_{\partial\overline{\Omega}} \mathrm{d}\Gamma\,. \tag{23}$$

This speed function $V_N(x)$ essentially represents a nonlocal version of the exact shape sensitivity (19). It serves in the Hamilton–Jacobi equation for a gradient descent solution for the structural optimization:

$$\frac{\partial\Phi}{\partial t} = V_N\,|\nabla\Phi| \ \text{ and } \ \left.\frac{\partial\Phi}{\partial N}\right|_{\partial\overline{\Omega}} = 0\,. \tag{24}$$

The reader is referred to Wang *et al.* (2003) for a detailed proof of this derivation. Finally, we can describe our optimization algorithm as an iterative process as follows:

Main Algorithm:

Step 1: Initialize the level-set function $\Phi\,(x,0)$ at $t = 0$, corresponding to an initial design Ω in terms of its boundary Γ.

Step 2: Compute the displacement field u and the adjoint displacement field w through the linear elastic system.

Step 3: Calculate the "speed function" $V_N(x)$ for x on the surface $\Phi(x)$ along the normal direction $N(x)$.

Step 4: Solve the level set (24) to update the embedding function $\Phi(x,t)$.

Step 5: Check whether a termination condition is satisfied. If the condition is met, then a convergent solution has been found. Otherwise, repeat Steps 2 through 5 until convergence. The termination condition is defined as

$$\int_{\overline{\Omega}} |V_N(x)|\,\delta(\Phi)\,|\nabla\Phi|\ \mathrm{d}\Omega\ \leq\ \gamma\,,$$

where γ is a specified error limit.

5
Level-set computations

There are a number of computational issues that are important to the proposed level-set method. At first glance, the technique seems to be expensive. By embedding the structural boundary as the level set of a higher dimensional function, a boundary curve of a two-dimensional problem is transformed into a surface, while a boundary surface of a general 3D solid has to be treated as a volumetric object. However, the level-set embedding is only defined at the particular zero set $\Phi(x,t) = 0$. This fact has been exploited to develop highly efficient algorithms that reduce the computational complexity back to the physical level of the structural boundary (Breen 2001; Sethian 1999). Further, a set of highly accurate and robust numerical algorithms has been developed for a discrete solution of the PDE of (24) (Osher 1988; Osher 2001; Peng 1999). In this section, we briefly describe some of the key aspects in the numerical implementation of the level-set method. In next section we present several developments

to further improve the computational speed, numerical accuracy and reliability.

5.1 Approximation of the level-set function

In the algorithm presented here, the geometric boundary of the structure under optimization is described as the zero level set of $\Phi(x,t)=0$. In its numerical implementation, the embedding function Φ may be represented in any convenient form. It is often described as a rectangular sampling on a rectilinear grid of x over $\overline{\Omega}$ (Osher 1988). Conventional interpolation functions may be used on a set of grid nodes, such as

$$\Phi(x,t)=\sum_i \Phi_i(t)N_i(x)\,, \tag{25}$$

where $\phi_i(t)$ are the nodal values of the level-set function and $N_i(x)$ describe the standard interpolation functions. The nodal values are updated during the optimization procedure (Wang *et al.* 2003).

In general, the linear elastic equation (10) may be solved by a finite element method. In the numerical implementation, functions $\delta(\Phi)$ and $H(\Phi)$ have to be approximated with a first-order accurate smoothed version such as defined in (Osher 1988, 2001). We use the following version (Wang *et al.* 2003):

$$H(\Phi)=\begin{cases} 0 & \Phi<-\xi \\ \dfrac{3}{4}\left(\dfrac{\Phi}{\xi}-\dfrac{\Phi^3}{3\xi^3}\right)+\dfrac{1}{2} & -\xi\le\Phi<\xi \\ 1 & \Phi\ge\xi \end{cases}, \tag{26}$$

where ξ is a parameter of choice to determine the size of the bandwidth of numerical smoothing. We found that a good value of ξ is between 0.5 and 0.7 times the minimum grid width $\Delta_{\min}$.

5.2 Up-wind computation schemes

The discrete solution to the Hamilton–Jacobi equation (24) is computed by using finite differences over discrete time steps and on a discrete grid over the level-set function. A highly robust and accurate computational method was developed by Osher and Sethian (1988) to address the problem of overshooting. Based on the notion of weak solutions and entropy limits, a so-called "up-wind scheme" is proposed to solve (24) with the following update equation:

$$\phi_{ijk}^{n+1}=\phi_{ijk}^{n}-\Delta t\left[\max(V_{N_{ij}},0)\nabla^{+}+\min(V_{N_{ij}},0)\nabla^{-}\right], \tag{27}$$

with

$$\nabla^{+}=\Big[\max\left(D_{ijk}^{-x},0\right)^2+\min\left(D_{ijk}^{+x},0\right)^2+\max\left(D_{ijk}^{-y},0\right)^2+\min\left(D_{ijk}^{+y},0\right)^2+\max\left(D_{ijk}^{-z},0\right)^2+\min\left(D_{ijk}^{+z},0\right)^2\Big]^{1/2},$$

$$\nabla^{-}=\Big[\max\left(D_{ijk}^{+x},0\right)^2+\min\left(D_{ijk}^{-x},0\right)^2+\max\left(D_{ijk}^{+y},0\right)^2+\min\left(D_{ijk}^{-y},0\right)^2+\max\left(D_{ijk}^{+z},0\right)^2+\min\left(D_{ijk}^{-z},0\right)^2\Big]^{1/2}.$$

Here, Δt is the time step, and $D_{ijk}^{\pm x}, D_{ijk}^{\pm y}$, and $D_{ijk}^{\pm z}$ are the respective forward and back difference operators in the three dimensions of $x\in\mathrm{R}^3$ for a general 3D solid. In addition, the time steps Δt must be limited to ensure the stability of the up-wind scheme (27). The Courant–Friedrichs–Lewy (CFL) condition requires Δt to satisfy $\Delta t\ \max|V_{N_{ijk}}|\le\Delta_{\min}$, where $\Delta_{\min}=\min(\Delta x,\Delta y,\Delta z)$ stands for the minimum grid space among the three dimensions (Osher 1988). Furthermore, in order to obtain highly accurate numerical results, the level-set function $\Phi(x,t)$ is often initialized as the signed distance function and to satisfy the Eikonal equation

$$|\nabla\Phi(x,t)|=1\,. \tag{28}$$

The first-order scheme is well known for its numerical stability. However, it is highly diffusive. It can be made higher order through a total-variation-diminishing (TVD) Runge–Kutta scheme (Shu 1988). A second-order method in time is given by Sethian (1999) as

$$\begin{cases} \tilde{\phi}_{ijk}^{n+1}=\phi_{ijk}^{n}-\Delta t\left[\max\left(V_{N_{ijk}}^{n},0\right)\nabla^{n+}+\min\left(V_{N_{ijk}}^{n},0\right)\nabla^{n-}\right] \\ \phi_{ijk}^{n+1}=\phi_{ijk}^{n}-\dfrac{\Delta t}{2}\left[\begin{matrix}\max\left(V_{N_{ij}}^{n},0\right)\nabla^{n+}+\min\left(V_{N_{ijk}}^{n},0\right)\nabla^{n-}+ \\ \max\left(\tilde{V}_{N_{ijk}}^{n+1},0\right)\tilde{\nabla}^{n+1}+\min\left(\tilde{V}_{N_{ijk}}^{n+1},0\right)\tilde{\nabla}^{n+1}\end{matrix}\right], \end{cases} \tag{29}$$

where $\tilde{V}_N$ is evaluated with the temporary value $\tilde{\phi}_{ijk}$. In addition, higher order space schemes for the space quantities ∇^{+} and ∇^{-} for the discrete approximation can be constructed with an essentially non-oscillatory (ENO) interpolation as fully described by Sethian (1999) and Shu and Osher (1988). Here, we shall omit their details for brevity. We have implemented these so-called "high-resolution" schemes and found that they are indeed more accurate than the first-order scheme as claimed in the literature.

5.3 Local schemes of level-set computation

The up-wind solutions produce the motion of level-set models over the entire range of the embedding, i.e., for

all values of Φ in (24). Since the optimum structural boundary is defined to be a single model, i.e., at $k = 0$, the calculation of solutions over the entire range of isovalues is unnecessary. This forms the basis for "narrow-band" schemes that solve (24) in a narrow band of the grid nodes that surround the level set of interest (Sethian 1999, 2000). While the up-wind scheme makes the level-set method numerically robust, the narrow-band scheme makes its computational complexity proportional to the boundary area of the structure being optimized rather than the size of the volume in which it is embedded. We reported the use of the narrow-band scheme in an earlier implementation of the level-set method in Wang *et al.* (2003).

Another an efficient method has been developed in Peng (1999) by making the embedding function Φ a distance function. Then, while the function Φ is maintained as a signed distance function, a local computation of the level set requires updates of only those points for which $\Phi \approx 0$. This *local computation scheme* is even simpler and more efficient. It has been shown that this method has a formal complexity of $O(N)$ in the 2D case and $O(N^2)$ in the 3D solid case, where N is the size of the spatial grid in each direction of the level set (Peng 1999). In other words, the complexity of the level-set model computation remains at the level of its physical dimension, not of the higher dimension of its embedding function. This advantage makes the local level-set method attractive from a practical standpoint.

5.4
Velocity extension and re-initialization of the level-set function

In the level-set formulation, we need the normal velocity V_N in a neighborhood of the design boundary or the zero level set $\Gamma(t)$. As suggested by Sethian (1999), the most natural way to extend V_N off the design boundary is to let the velocity V_N be constant along the curve normal to $\Gamma(t)$ such that

$$\nabla V_N \cdot \nabla \Phi = 0\,. \tag{30}$$

This leads to the following hyperbolic partial differential equation:

$$\frac{\partial V_N}{\partial t} + S(\Phi)\frac{\nabla \Phi}{|\nabla \Phi|} \cdot \nabla V_N = 0\,, \tag{31}$$

where $S(\Phi)$ is the signature function of Φ defined as

$$S(\Phi) = \begin{cases} -1 & \text{if } \Phi < 0 \\ 0 & \text{if } \Phi = 0 \\ +1 & \text{if } \Phi > 0 \end{cases}. \tag{32}$$

In order to increase the regularity, $S(\Phi)$ may be approximated by $\Phi/\sqrt{\Phi^2 + \Delta_{\min}^2}$. Accurate and robust numerical schemes, such as the first-order up-wind method, exist to compute discrete solutions to the partial differential equation of velocity extensions (Peng 1999). For simplicity of the presentation, the reader is referred to Osher (2001) and Peng (1999) for detailed formulae.

Another important consideration in the local computation of zero level sets is re-initialization of the level-set function (Sethian 1999). In most cases, it is impossible to prevent $\Phi(x, t)$ from deviating away from a signed distance function. Flat or steep regions may develop as the boundary moves, rendering computation of the normal vector, normal velocity, and curvature at the places inaccurate. This would result in inaccurate design boundaries. For numerical reasons, the level-set function needs to be resurrected to be close to a signed distance function from time to time (Peng 1999; Sethian 1999). We use another PDE-based method for this purpose by solving the following Hamilton–Jacobi equation to its steady state:

$$\frac{\partial \Phi}{\partial t} = S(\Phi_0)(1 - |\nabla \Phi|)\,, \tag{33}$$

which results in the desired signed distance function of $S(\cdot)$ (Sethian 1999). This approach allows us to avoid finding the design boundary explicitly. As reported in the literature, a first-order discrete time up-wind scheme with a second-order essentially non-oscillatory (ENO) discrete space scheme would again yield good results (Osher 2001; Shu and Osher 1988).

5.5
Curvature discretizion

In the numerical implementation of a three-dimensional case, we need to approximate the normal N and the mean curvature $\kappa = \nabla \cdot N$ of the surface boundary:

$$N = -\frac{\nabla \Phi}{|\nabla \Phi|} = -\begin{bmatrix} \Phi_x \Big/ \sqrt{\Phi_x^2 + \Phi_y^2 + \Phi_z^2} \\ \Phi_y \Big/ \sqrt{\Phi_x^2 + \Phi_y^2 + \Phi_z^2} \\ \Phi_z \Big/ \sqrt{\Phi_x^2 + \Phi_y^2 + \Phi_z^2} \end{bmatrix}, \tag{34}$$

$$\kappa = -\frac{\begin{array}{r}\left(\Phi_y^2 + \Phi_z^2\right)\Phi_{xx} + \left(\Phi_x^2 + \Phi_z^2\right)\Phi_{yy} + \left(\Phi_x^2 + \Phi_y^2\right)\Phi_{zz} - \\ 2\Phi_x\Phi_y\Phi_{xy} - 2\Phi_y\Phi_z\Phi_{yz} - 2\Phi_z\Phi_x\Phi_{zx}\end{array}}{\left(\Phi_x^2 + \Phi_y^2 + \Phi_z^2\right)^{1.5}} \tag{35}$$

We compute the value of κ at grid points neighboring the zero level set and then interpolate its value on the design boundary whenever it is needed. In the discrete computation, $\kappa, \Phi_x, \Phi_y, \Phi_z, \Phi_{xx}, \Phi_{yy}$, and Φ_{zz} are all discretized by central difference, given as

$$(\phi_{xy})_{ijk} = \frac{\phi_{i+1j+1k} - \phi_{i+1j-1k} - \phi_{i-1j+1k} + \phi_{i-1j-1k}}{4\Delta x \Delta y},$$

$$(\phi_{yz})_{ijk} = \frac{\phi_{ij+1k+1} - \phi_{ij+1k-1} - \phi_{ij-1k+1} + \phi_{ij-1k-1}}{4\Delta y \Delta z},$$

$$(\phi_{zx})_{ijk} = \frac{\phi_{i+1jk+1} - \phi_{i-1jk+1} - \phi_{i+1jk-1} + \phi_{i-1jk-1}}{4\Delta z \Delta x}. \tag{36}$$

In order to enhance the robustness of the algorithm, we further confine the scope of the mean curvature as follows:

$$\kappa_{ijk} = \min\left(\Delta_{\min}, \max\left(\kappa_{ijk}, -\Delta_{\min}\right)\right). \tag{37}$$

This means that the minimum approximate value of the level-set curvature is stipulated as the minimum grid width.

5.6 Recovery of the level sets

In the level-set-based framework presented here, the geometric boundary of the structure under optimization is implicitly described as the zero level set of $\Phi(x,t) = 0$. There is no need to explicitly recover the boundary until the end of the optimization. There exist many techniques in most of the popular scientific software systems to compute iso-curves and iso-surfaces, essentially 2D and 3D level sets. For example, it is often convenient to describe the embedding function Φ as a rectangular sampling on a rectilinear grid of x over $\overline{\Omega}$ (Sethian 1999). Then, the well-known marching-cubes technique in computer graphics can be directly applied to compute the zero level set of the optimal solution.

6 Enhancements of level-set evolution

In this section we present two enhancements to further improve the computational speed, numerical accuracy, and reliability.

6.1 Conjugate mapping of the moving velocity

It is well known that the gradient descent method is not particularly efficient in the family of optimization methods. A significant improvement is to modify the gradient descent direction by a positive definite matrix approximating the Hessian matrix, namely, the conjugate gradient method. As for the infinite-dimensional problem (15), it is difficult to construct such a similar function. Here we present a heuristic method aimed at improving the descent direction according the problem characteristics. The basic idea is to increase the difference of the velocity along the moving boundary while keeping the objective function descent. As a result, the speed of convergence of the PDE-based optimization will be increased.

This heuristic idea requires us to define a conjugate mapping function $f(\cdot)$ that satisfies the following conditions:

1) f is continuous and closed in the tangential space T of the active constraint: $f(r) \in C^0$ and $f(r) \in T$ for $\forall r \in T$.
2) f is an odd function: $f(-r) = -f(r)$.
3) f is a non-decreasing function: $f'(r) \geq 0$.

It is not trivial to find a function satisfying these conditions. Here, we use the following procedure. First, we choose a nonlinear function $F(r)$ that satisfies conditions (b) and (c). Then, we let $F(r)$ project on the tangential

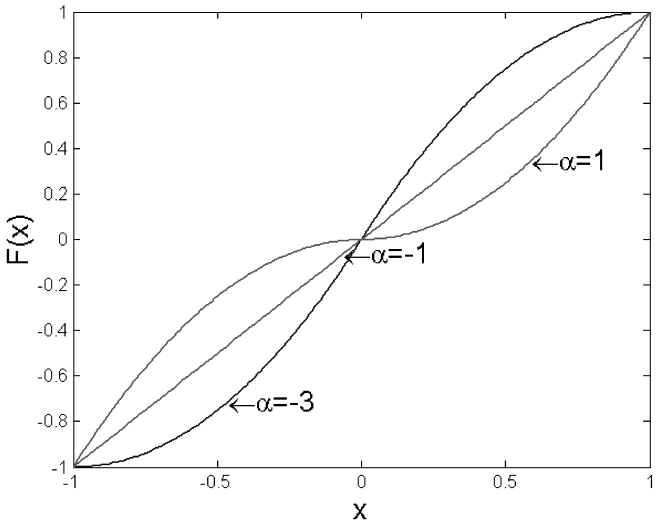

Fig. 2 A conjugate mapping function for the velocity field function

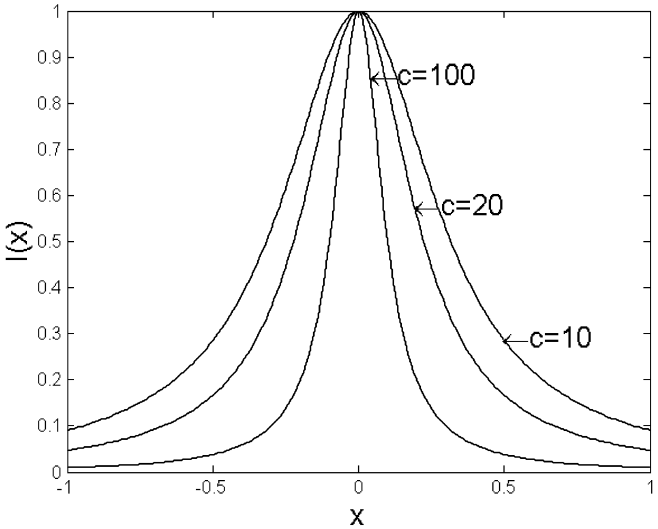

Fig. 3 Weighting function for fairing and smoothing the level sets

space T of the active constraint. Thus, a conjugate mapping function is constructed as follows:

$$f(V_n) = F(V_n) - \mu \quad \text{for} \quad V_n \in T\,, \tag{38}$$

where μ is the average of the velocity function $F(V_n)$ along the entire design boundary Γ. As derived by Wang *et al.* (2003) in detail, it is given as

$$\mu = \int\limits_{\partial\overline{\Omega}} F(V_n)\,\mathrm{d}\Gamma \Bigg/ \int\limits_{\partial\overline{\Omega}} \mathrm{d}\Gamma\,. \tag{39}$$

With this nonlinear mapping function, the Hamilton–Jacobi equation (24) can be modified as

$$\frac{\partial\Phi}{\partial t} = f(V_n)\,|\nabla\Phi|\,,$$

$$\left.\frac{\partial\Phi}{\partial N}\right|_{\Gamma} = 0\,. \tag{40}$$

It can also be shown that the PDE generates a gradient descent solution to the problem of optimization (17) as the original PDE (24) such that $\mathrm{d}J(u,\Phi)/\mathrm{d}t \le 0$. A proof essentially follows the proof for the original PDE (24) as presented in our earlier work (Wang *et al.* 2003). We shall omit the details here. It is also trivial to show that $f(r)$ is an odd function due to the fact that $F(r)$ satisfies condition (b). However, function $f(r)$ constructed by using (30) is not assured to fulfill condition (c). When this happens, the conjugate mapping of the velocity function may have a negative effect on the speed of convergence.

In our numerical implementation, we have used the following function $F(r)$ as illustrated in Fig. 2:

$$F(r) = r\left(\frac{1-\alpha}{2} + \frac{1+\alpha}{2}\,|r|\right)\,, \tag{41}$$

where α is a constant. In our numerical experience with examples to be presented in the next section, we have found that this nonlinear mapping improves the computing efficiency significantly (by 2–3 times) compared with the direct gradient descent method.

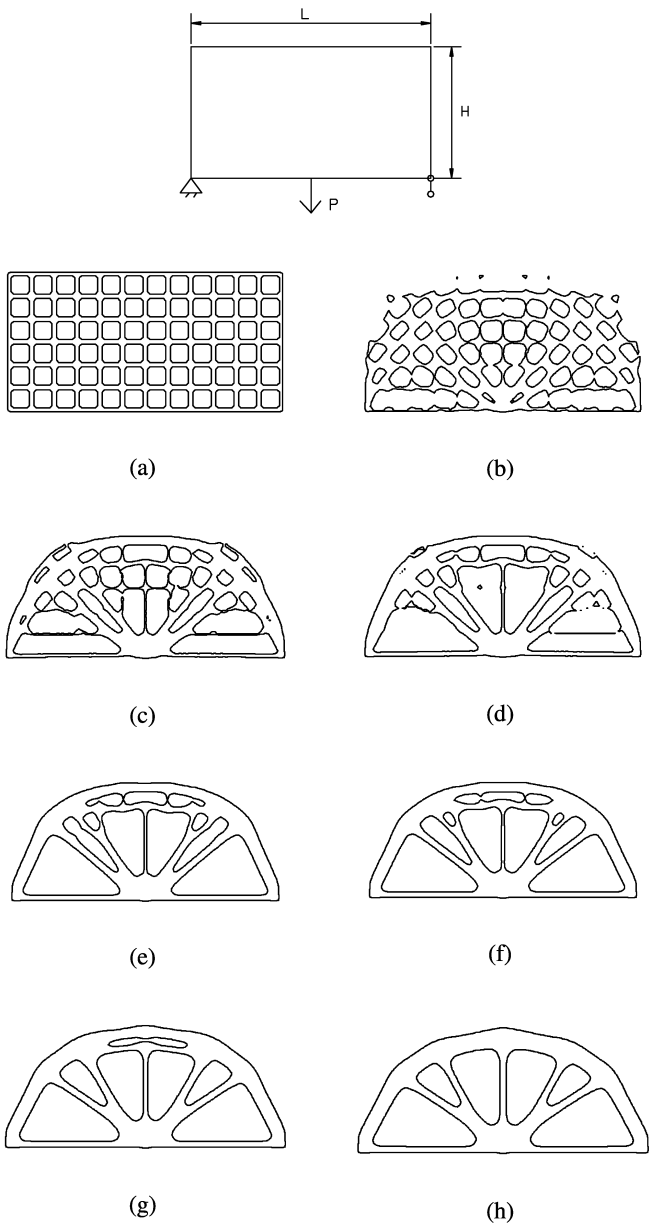

Fig. 4 A Michell-type structure with fixed–simple supports. (a) Initial design. (b)–(g) Intermediate results. (h) Final solution

6.2 Variational regularization of the level sets

During the course of shape optimization with the level-set models, it is possible that the boundary may not be able to maintain a certain level of smoothness due to numerical errors of the discrete solutions. It is highly desirable that the irregularities be removed to enhance the

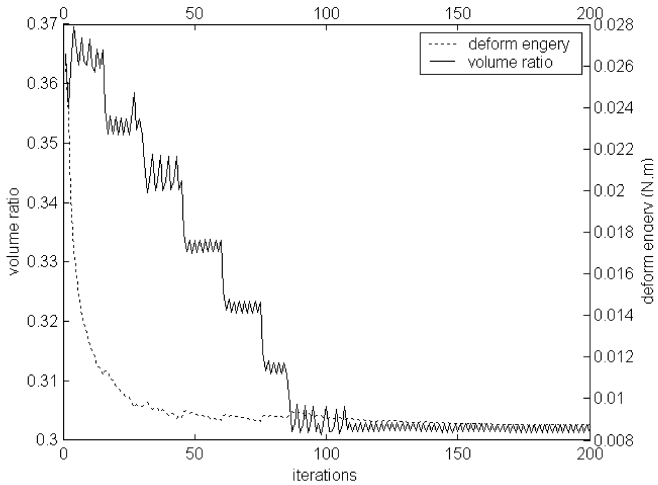

Fig. 5 The changes in the mean compliance and the volume of the structure with iteration for the example in Fig. 4

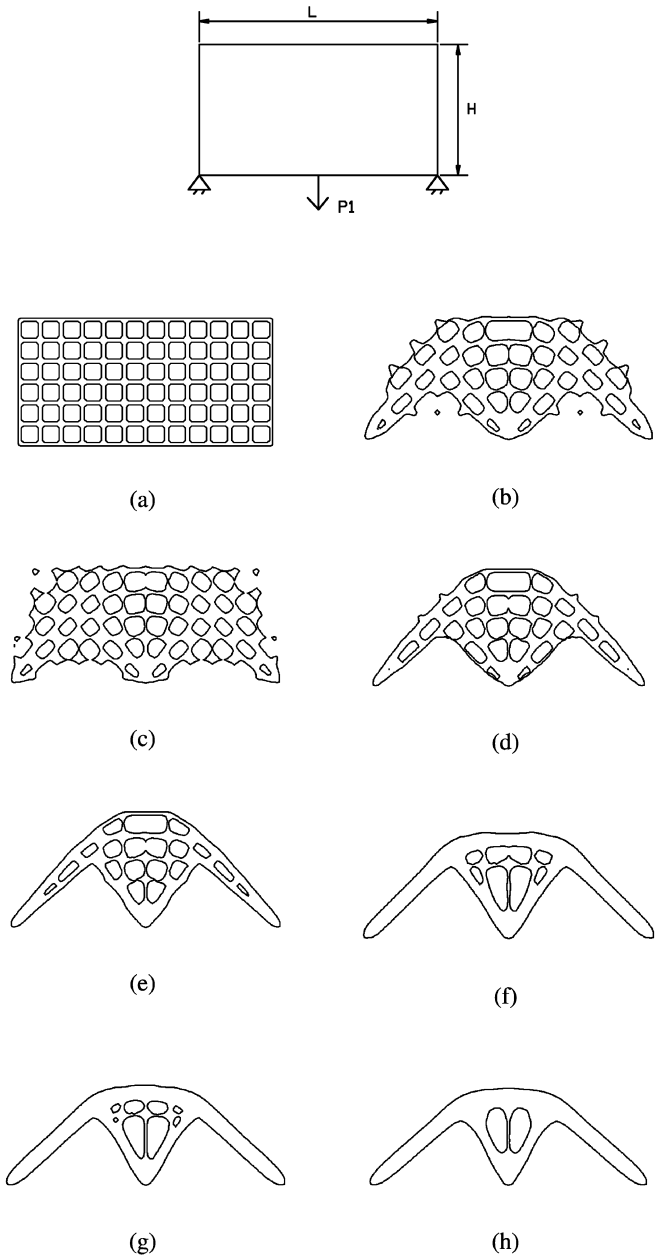

Fig. 6 A Michell-type structure with fixed–fixed supports. (a) Initial design. (b)–(g) Intermediate results. (h) Final solution

fidelity of the level sets, while the meaningful discontinuities in the boundary representing topological changes are kept. This is similar to the problem of "denoising" in image processing (Sapiro 2001; Sethian 1999). This function can be easily incorporated into the implicit boundary framework, again due to the flexibility of the level-set methods.

The regularization problem is defined as a variational problem (Sapiro 2001). We introduce a weighted length or area of the level set, namely,

$$E_S(\Phi) = \int_{\Gamma} I(x)\,\mathrm{d}\Gamma = \int_{\overline{\Omega}} I(x)\delta(\Phi)\,|\nabla\Phi|\,\mathrm{d}\Omega\,, \tag{42}$$

where $I(x) > 0$ corresponds to a Riemman metric. Thus, the objective function of the optimization problem (15) is modified as

$$\overline{J}(u,\Phi) \;=\; \int_{\overline{\Omega}} F(u)H(\Phi)\,\mathrm{d}\Omega + E_S(\Phi)\,. \tag{43}$$

Again, taking the Fréchet derivative of this objective function with respect to Φ as in the original case, we obtain the gradient of the new objective function (43) at the zero level sets as follows:

$$\overline{\beta}(u,w,\Phi) = \beta(u,w,\Phi) - \nabla\cdot\left(I(x)\frac{\nabla\Phi}{|\nabla\Phi|}\right) =$$

$$\beta(u,w,\Phi) - I(x)\nabla\cdot\left(\frac{\nabla\Phi}{|\nabla\Phi|}\right)\,. \tag{44}$$

This corresponds to the total variation including regularization. The reason to use this variation form is straightforward. Here, the term $\nabla\cdot(\nabla\Phi/|\nabla\Phi|)$ is the mean curvature κ of the level set. It is well known that a surface moving in its normal direction with the mean curvature as the velocity, also called the mean curvature flow, converges to the minimal surface. The mean curvature flow is also interpreted in the literature as an anisotropic diffusion (Sapiro 2001), and it diffuses only in the tangential direction of the surface. Therefore, the regularization term in (42) plays a role in fairing the level sets only without any effect on their normal motion.

The regularization variation of (42) may be replaced by the so-called weighted total variation energy (Osher 2001; Sapiro 2001)

$$E_{TV}(\Phi) = \int_{\overline{D}} I(x)\,|\nabla\Phi|\,\mathrm{d}\Omega\,, \tag{45}$$

with $I(x)$ being regarded as the weighting coefficients. By deriving the Fréchet derivative for $E_{TV}(\Phi)$ with respect to Φ, we will obtain the same gradient of the objective

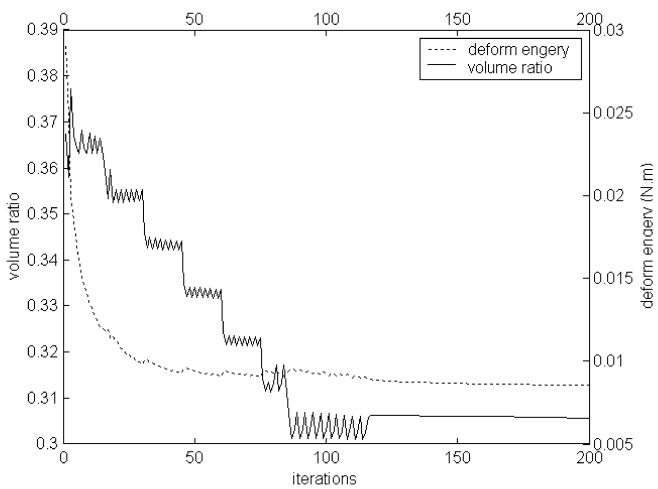

Fig. 7 The changes in the mean compliance and the volume of the structure with iteration for the example in Fig. 6

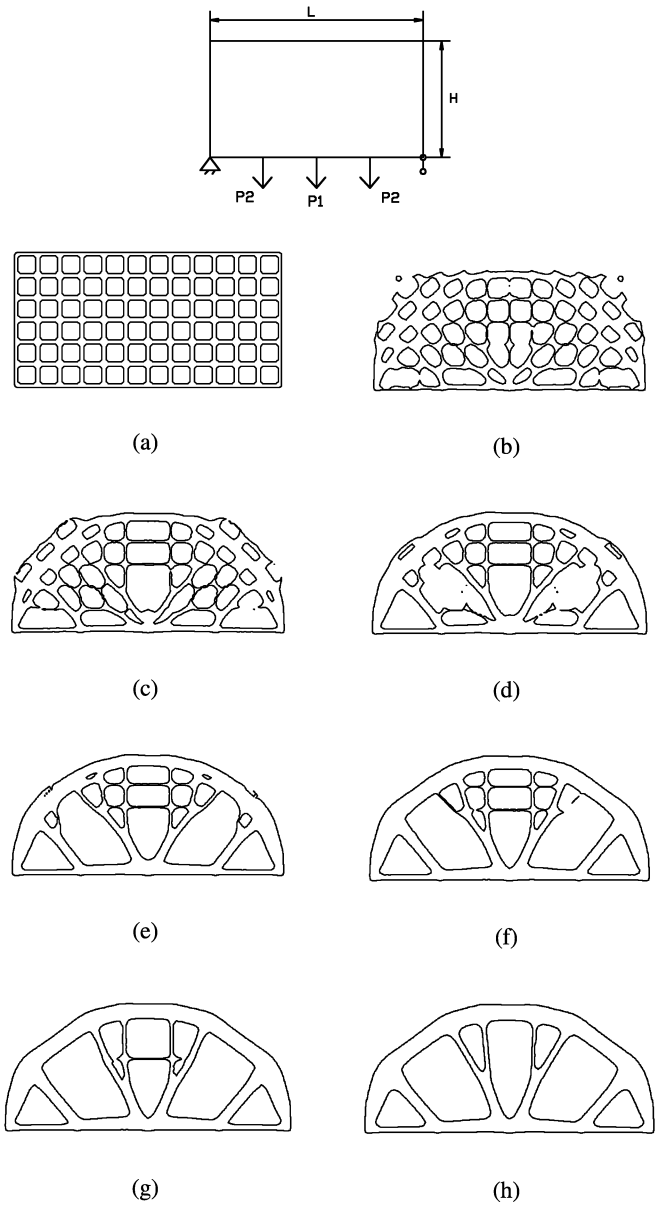

Fig. 8 A Michell-type structure with fixed–simple supports and multiple loads $P_1 = 30$ N and $P_2 = 15$ N. (a) Initial design. (b)–(g) Intermediate results. (h) Final solution

function as (44). Thus, the variational regularization developed here can also be used to reduce the total variation of the level sets.

The geometric metric $I(x)$ is chosen according to the following criteria: (1) The regularization term in (44) should not have any significant influence on the process of optimization defined by the velocity function $V_N(x)$. (2) As the level set moves to approach the optimum, the regularization must be enhanced gradually so as to obtain a smoothing or fairing of the structure boundary. In this study, we use the geometric metric as follows:

$$I(x) = \frac{c_1}{1 + c_2 V_N^2(x)}\,, \tag{46}$$

where c_1 and c_2 are two positive constants used to shape the weighting function as shown in Fig. 3.

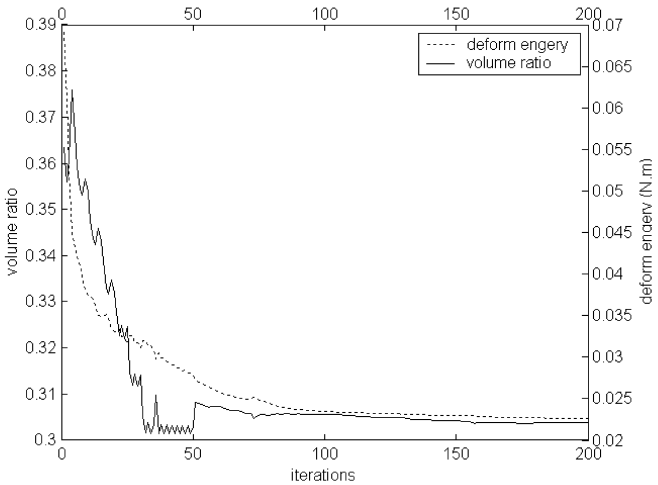

Fig. 9 The changes in the mean compliance and the volume of the structure with iteration for the example in Fig. 8

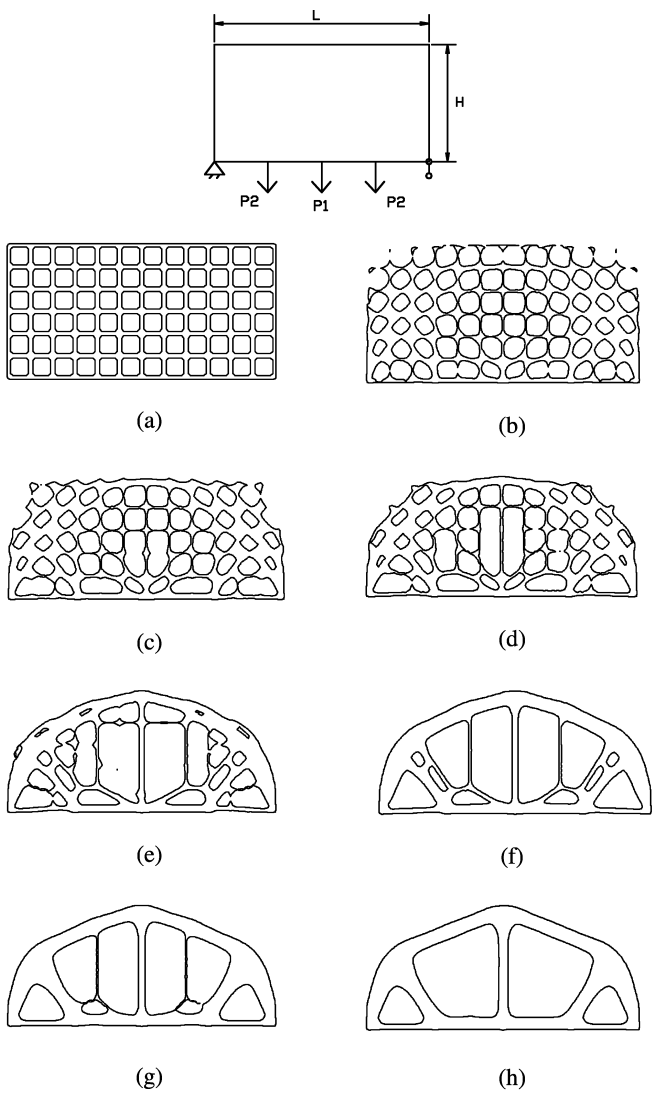

Fig. 10 A Michell-type structure with fixed–simple supports and multiple loads $P_1 = 30$ N and $P_2 = 30$ N. (a) Initial design. (b)–(g) Intermediate results. (h) Final solution

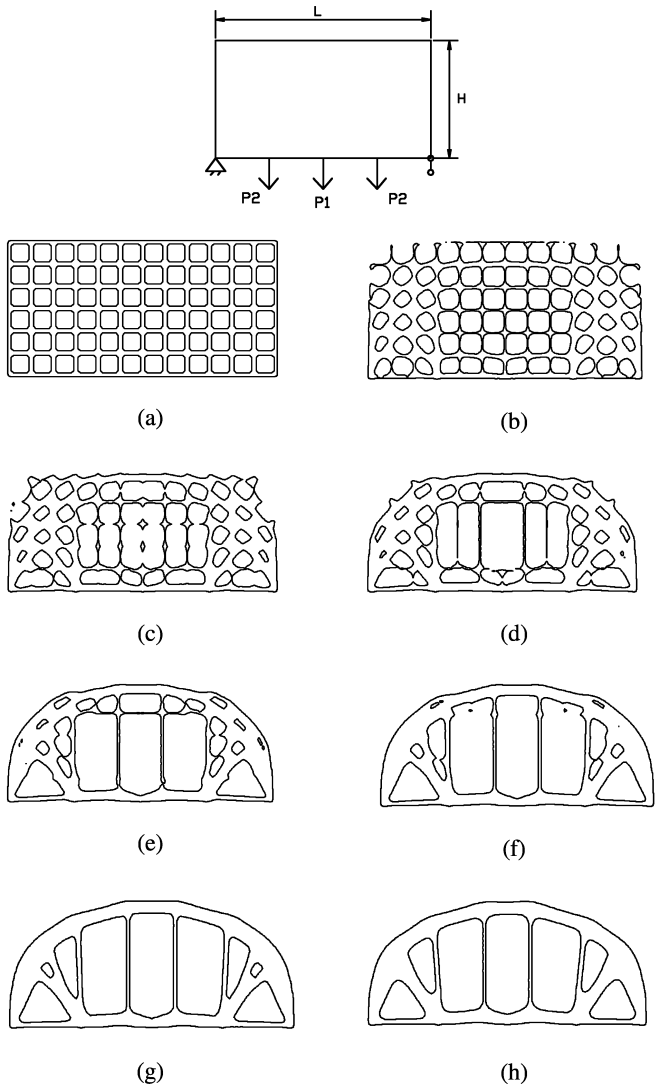

Fig. 11 A Michell-type structure with fixed–simple supports and multiple loads $P_1 = 20\,\mathrm{N}$ and $P_2 = 40\,\mathrm{N}$. (a) Initial design. (b)–(g) Intermediate results. (h) Final solution

7
Numerical examples

In this section we present several examples of structural optimization obtained with the proposed algorithm and implementation. The optimization problem of choice is the mean compliance problem that has been widely studied in the relevant literature (e.g., Bendsoe 1997; Rozvany 1988). The objective function of the problem is the strain energy of the structure with a material volume constraint, i.e.,

$$J(u) = \int_D E_{ijkl}\varepsilon_{ij}(u)\varepsilon_{kl}(u)\,\mathrm{d}\Omega\,. \tag{47}$$

For all examples, the material used is steel with a modulus of elasticity of 200 GPa and a Poisson's ratio of $v = 0.3$. For clarity in presentation, the examples are in 2D under plane-stress conditions.

7.1
Michell-type structures

A Michell-type structure is first considered with a single load. A rectangular design domain of length L and height H with a ratio of $L : H = 12 : 6$ is loaded vertically at the center point of its bottom with $P = 30\,\mathrm{N}$ as shown in Fig. 4. The left bottom corner of the beam is fixed, while it is simply supported at the right bottom corner. A volume ratio of 0.3 is considered. The initial design and some intermediate and the final optimization results are shown in Fig. 4. The final optimum solution is nearly identical to what other researchers have obtained by using a homogenization-based method (see Bendsoe 1997; Rozvany 1988). A mesh of 62×122 quadrilateral elements is used for the finite element analysis, and the numerical width ξ for the approximate Heaviside function is chosen to be 0.7 times the grid width.

In the example, 72 holes are uniformly distributed in the initial design as shown, representing an original

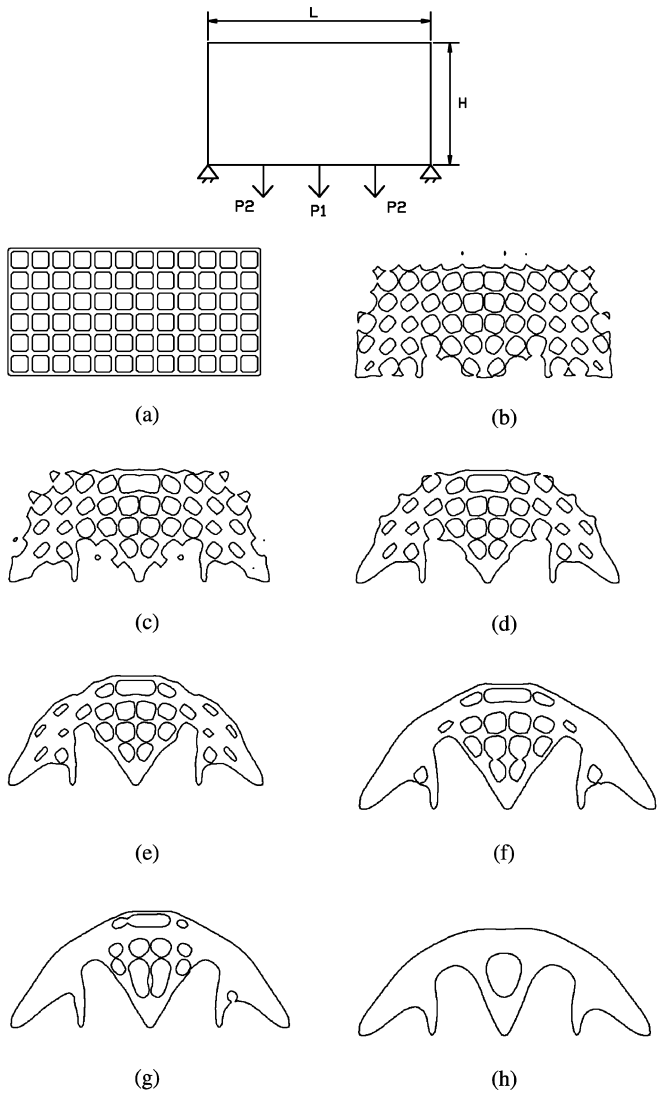

Fig. 12 A Michell-type structure with fixed–fixed supports and multiple loads $P_1 = 30\,\mathrm{N}$ and $P_2 = 15\,\mathrm{N}$. (a) Initial design. (b)–(g) Intermediate results. (h) Final solution

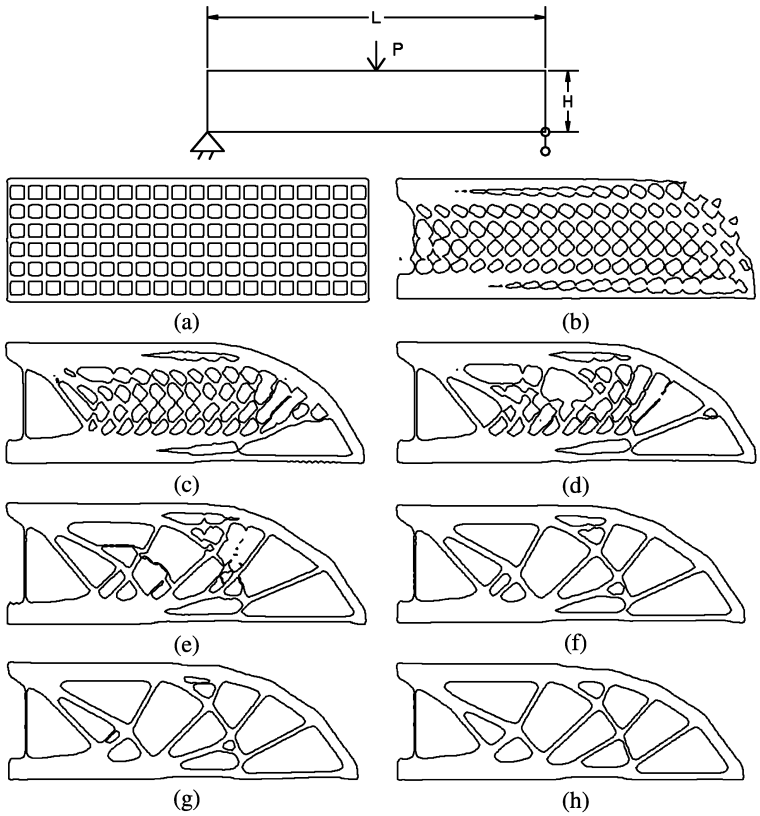

Fig. 13 A mid-point loaded beam (MBB beam) with fixed–simple supports and a volume ratio of 0.355. (a) Initial design. (b)–(g) Intermediate results. (h) Final solution

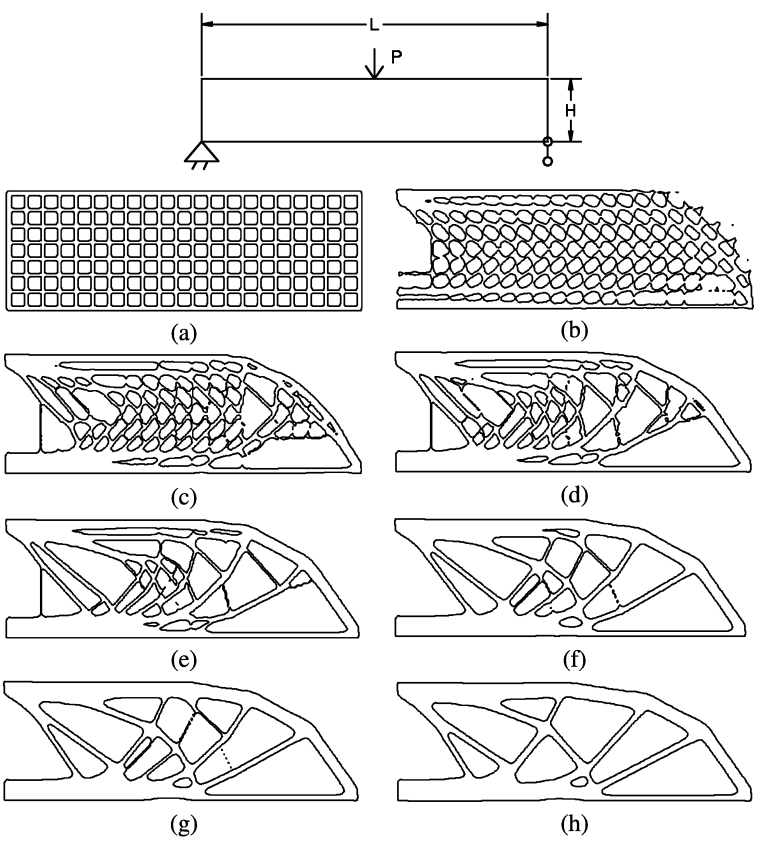

Fig. 14 A mid-point loaded beam (MBB beam) with fixed–simple supports and a volume ratio of 0.35. (a) Initial design. (b)–(g) Intermediate results. (h) Final solution

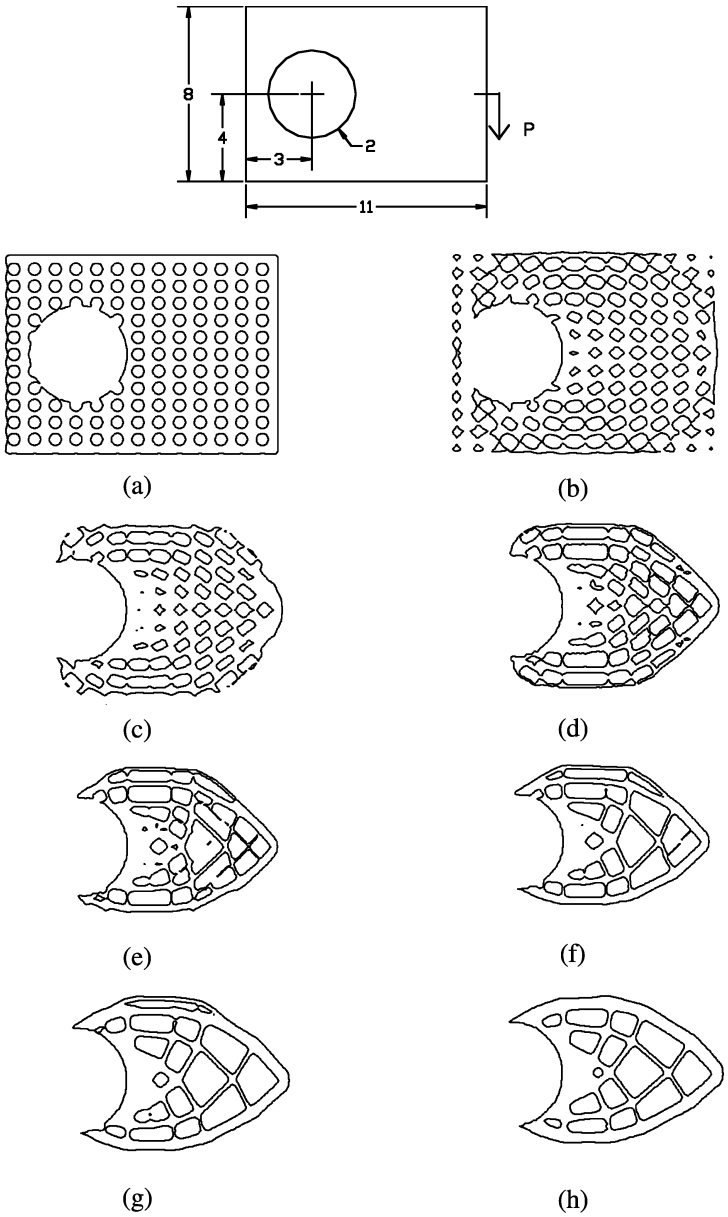

Fig. 15 The first Michell truss example. (a) Initial design. (b)–(g) Intermediate results. (h) Final solution

perforated structure. During the process of optimization, many of these holes merge, yielding "Swiss-cheese" structures during iteration. Many of the "Swiss-cheese" holes are gradually "gobbled up" by the level-set processing. In the intermediate steps, some pieces of the structure may also break off to become separated. However, they eventually evolve to disappear, since they are physically meaningless. This illustrates the flexibility and power of the level-set model in handling drastic topological changes. The convergence of the optimization process is shown with the changes with iteration of the objective function and the structure volume in Fig. 5.

The second example is similar to the first example, except that the right bottom corner support is also fixed and its volume ratio is 0.2. The initial design and some intermediate and the final optimization results are shown in Fig. 6 and the changes of the objective function and the structure volume with iteration are shown in Fig. 7.

7.2 Michell-type structures with multiple loads

A Michell-type structure is now considered with multiple loads at its bottom as shown in Fig. 8. The volume ratio is 0.3. Again, the mesh of 62×122 quadrilateral elements is used for FEM analysis. In Fig. 8, the structure has a fixed and a simple support at the bottom corners with $P_1 = 30\,\mathrm{N}$ and $P_2 = 15\,\mathrm{N}$. The initial design and some intermediate and the final optimization results are shown. Changes in the mean compliance and the body volume during iterations of the optimization are shown in Fig. 9. Figures 10–11 show the initial design and some intermedi-

ate and the final optimization results for three more cases of different values of loads of the example.

The third example of the Michell-type structure is similar to the example of Fig. 8, except that the supports are both of fixed type. The volume ratio is 0.3, and the loads are $P_1 = 30\,\mathrm{N}$ and $P_2 = 15\,\mathrm{N}$. The optimization results are shown in Fig. 12.

7.3 MBB beams

This example is said to be related to a problem of designing a floor panel of a passenger airplane, in Germany known as Messerschmitt–Bolkow–Blohm (MBB) beams. The floor panel is loaded with a concentrated vertical force $P = 80\,\mathrm{N}$ at the center of the top edge. It has a fixed support and a simple support at its bottom corners respectively. The design domain has a length-to-height ratio of 24 : 4. We use 56×165 quadrilateral elements to model a half of the structure, due to the geometric symmetry. The numerical width ξ of the Heaviside function is taken as 0.5 times the grid width.

In Fig. 13 the volume ratio is specified to be 0.355, and the optimization results are shown. In Fig. 14, the volume ratio is slightly less than 0.35. As shown, the optimal design has a different topology with a smaller number of holes compared with the optimal design of Fig. 13 for the slightly higher volume ratio of 0.355.

7.4 The Michell trusses

The problem of Michell truss optimization is presented here. The design domain is shown in Fig. 15. An optimum structure is to be designed to transfer a vertical force to the circular fixed support. A force $P = 20\,\mathrm{N}$ is applied to the middle of the right side. A mesh of 112×82 quadrilateral elements is used, the volume ratio is constrained to be 0.165, and the numerical width ξ is specified to be 0.5 times the minimum grid width. The optimization results of the example are shown in Fig. 15. Another example of the Michell truss is shown in Fig. 16 with a different boundary condition and the same load of $P = 20\,\mathrm{N}$. The volume ratio is constrained at 0.2. The FEM analysis uses a mesh of 86×86 quadrilateral elements.

7.5 Cantilever beams

A cantilever beam of ratio 3.2 : 2 is loaded vertically at the center of its free end with a force of 80 N as shown in Fig. 17. A volume ratio constraint of 0.25 is considered. The design domain is discretized using 22×34 quadrilateral elements. Two different values of ξ are used for the smoothing of Heaviside function. The optimization results are shown in Figs. 17 and 18.

In Fig. 17, $\xi = 1.0$ is used. This means that the smoothing width for the Heaviside function is equal to the minimum grid width of the finite elements. In Fig. 18, a tighter width is used, $\xi = 0.75$. From the figures it is evident that both optimization processes arrive at the same final optimal solution, starting with the same initial design as shown. However, these two processes undertake different intermediate steps or optimization paths.

It is interesting to point out that in Fig. 18, with the tighter numerical width, an intermediate solution (Fig. 18e) is achieved. This intermediate design is very similar to optimal solutions that are often reported in the literature, especially those obtained with a homogenization (or SIMP) approach. In our process of optimization based on the level-set models, the shape of the structure continues to evolve to approach to the final result shown in Fig. 18h. The final solution has a very different topology from the intermediate solution, with a slight improvement in the mean compliance. This case shows that

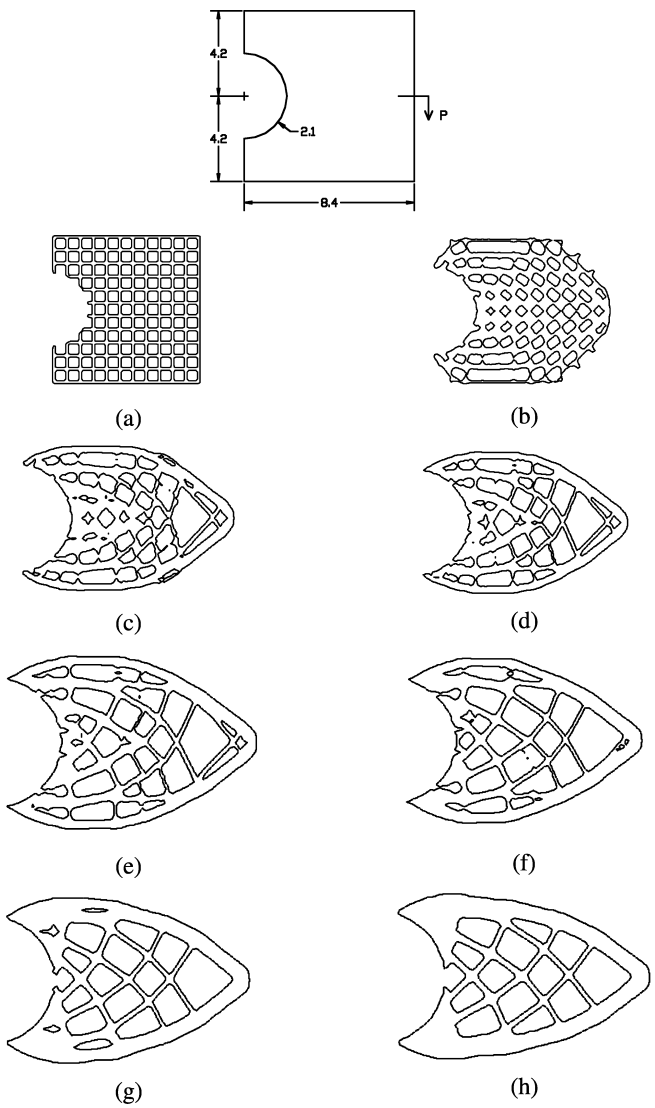

Fig. 16 The second Michell truss example. (a) Initial design. (b)–(g) Intermediate results. (h) Final solution

the problem of optimal topology may become very sensitive and multiple solutions may exist.

7.6 Computational time

Based on the numerical examples presented above, we further discuss the computational performance of the level-set-based method described above. There are two major computational tasks in the course of optimization. The first is the physical problem of the linear elastostatic system of the solid structure. The underlying field equations are solved with the finite element method. The second task is the computation of the movements of the level sets to describe the changes in structural shape. For the examples that are examined, we found that it generally takes 80–250 iterations for an accurate optimal solution. The use of the nonlinear mapping of the velocity function can reduce the iteration number by about 2.5 times when compared with a direct use of the velocity function as reported in our earlier work (Wang *et al.* 2003).

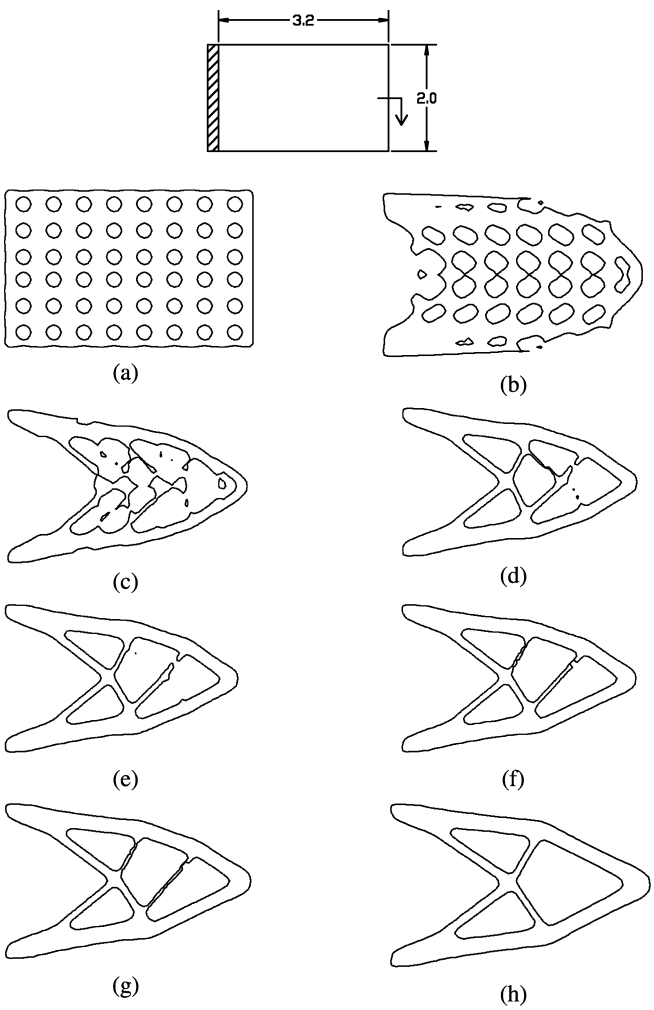

Fig. 17 The first cantilever example with $\xi = 1.0$. (a) Initial design. (b)–(g) Intermediate results. (h) Final solution

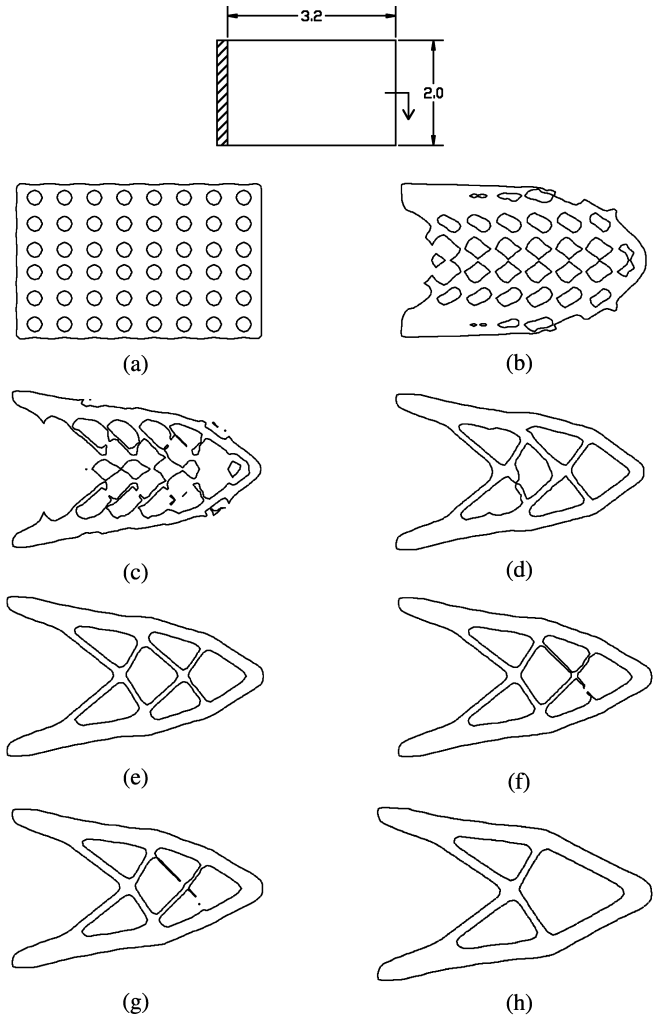

Fig. 18 The second cantilever example with $\xi = 0.75$. (a) Initial design. (b)–(g) Intermediate results. (h) Final solution

Table 1 Comparison of the computing time for the cantilever beam examples

Element Number	9184	2772	1364	748
FEA Time (s)	45.93	8.232	3.618	1.952
Level Set Time (s)	0.659	0.113	0.054	0.030
Level Set / Total	1.41%	1.35%	1.47%	1.51%

Furthermore, it is experienced that the FEM analysis takes the major portion of the total computational time and the level-set updating uses only a small fraction. For the cantilever beam example, Table 1 tabulates the CPU time (in seconds) used in each iteration for the tasks of the level-set updates and the FEM analysis for four different mesh sizes. It shows that the level-set computation takes between 1.35% to 1.51% of the total computing time. Clearly, the level-set method shows its high efficiency. It also shows that the local level-set computation method employed has a computing behavior of the linear complexity, as predicted.

8 Conclusions

We have presented a region framework for structural shape and topology optimization based on the level-set methods. As a boundary optimization problem, the structure is implicitly represented with a level-set model that is embedded in a scalar function. The dynamics of the level-set function is governed by a simple Hamilton–Jacobi convection equation. The movement of the moving boundaries of the structure is driven by a transformation of the objective and the constraints into a speed function that defines the level-set propagation. The result is a 3D structural optimization technique that demonstrates outstanding flexibility in handling topological changes, the fidelity of boundary representation, and the degree of automation, comparing favorably with other methods in the literature based on explicit boundary variation or homogenization.

A number of numerical techniques for an efficient and robust implementation of the proposed method are described, including using a local computation scheme to keep the computational complexity linear with the complexity of the physical boundary of the structure, while a second-order discrete method based on the TVD Runge–Kutta scheme is used for accurate and stable numerical solution. We have developed two techniques for further enhancement of the level-set computations. A technique of conjugate velocity mapping is described to substantially increase computational efficiency from the conventional gradient descent method for a faster convergence. The concept of variational regularization with an anisotropic diffusion of the mean curvature flow is utilized to maintain the boundary smoothness without sacrificing its fidelity to topology. The proposed approach is tested with several examples of mean compliance optimization of a linear elastic structure, as they have been widely analyzed in the literature. The approach can certainly be applied to other problems of structural optimization involving multi-materials (Wang and Wang 2003).

The work presented in this paper is by no means complete. Our current algorithm is capable of creating new holes only from the Dirichlet boundary as reported by Allaire (2002), Wang *et al.* (2003), and Wang and Wang (2003). The creation process is typically slow. The level-set models are at ease in handling topological changes of merging or canceling holes. Therefore, the algorithm described here is efficient in performing topology optimization if a number of holes exist in the initial design. An immediate need is to develop a technique for the creation of holes as they are needed. In fact, the concept of "topological derivatives" has been discussed in the literature recently (Sokolowski 1999), and it seems to have a close connection with the concept of the "characteristic function" of the bubble method (Eschenauer 1994, 1997; Lewinski 1999). Thus, its application would add a significant "nucleation" capability to the level-set-based implicit moving boundary framework. It is foreseeable that our proposed optimization system based on this framework would able to generate, split, merge, or diminish holes or cavities within the structure as well as to move the interior and exterior boundaries to ultimately achieve an optimal design. Our preliminary investigation in this direction is promising and we shall report our complete results separately.

Acknowledgements This research work is supported in part by the USA National Science Foundation (NSF) (CMS-9634717), the Hong Kong Research Grants Council (Project No. CUHK4164/03E), and the Natural Science Foundation of China (NSFC) (Project No. 50128503 and 50390063).

References

Allaire, G. 1997: The homogenization method for topology and shape optimization. In: Rozvany, G. (ed.) *Topology Optimization in Structural Mechanics*, pp. 101–133

Allaire, G.; Jouve, F.; Taoder, A.-M. 2002: A level-set method for shape optimization. *C. R. Acad. Sci. Paris*, Ser. I **334**, 1–6

Bendsoe, M.P. 1989: Optimal shape design as a material distribution problem. *Struct. Optim.* **1**, 193–202

Bendsoe, M.P. 1997: *Optimization of Structural Topology, Shape and Material*. Berlin: Springer

Bendsoe, M.P. 1999: Variable-topology optimization: Status and challenges. In: Wunderlich, W. (ed.) *Proceedings of the European Conference on Computational Mechanics* (held in Munich, Germany)

Bendsoe, M.P.; Haber, R. 1993: The Michell layout problem as a low volume fraction limit of the homogenization method for topology design: an asymptotic study. *Struct. Optim.* **6**, 63–267

Bendsoe, M.P.; Kikuchi, N. 1988: Generating optimal topologies in structural design using a homogenisation method. *Comput. Methods Appl. Mech. Eng.* **71**, 197–224

Bendsoe, M.P.; Sigmund, O. 1999: Material interpolations in topology optimization. *Arch. Appl. Mech.* **69**, 635–654

Breen, D.; Whitaker, R. 2001: A level set approach for the metamorphosis of solid models. *IEEE Trans. Visual. Comput. Graphics* **7**(2), 173–192

Bulman, S.; Sienz, J.; Hinton, E. 2001: Comparisons between algorithms for structural topology optimization using a series of benchmark studies. *Comput. Struct.* **79**, 1203–1218

Diaz, A.R.; Bendsoe, M.P. 1992: Shape optimization of structures for multiple loading conditions using a homogenization method. *Struct. Optim.* **4**, 17–22

Eschenauer, H.A.; Kobelev, H.A.; Schumacher, A. 1994: Bubble method for topology and shape optimization of structures. *Struct. Optim.* **8**, 142–151

Eschenauer, H.A.; Schumacher, A. 1997: Topology and shape optimization procedures using hole positioning criteria. In: Rozvany, G. (ed.) *Topology Optimization in Structural Mechanics*, pp. 135–196. Wien: Springer

Lewinski, T.; Sokolowski, J.; Zochowski, A. 1999: Justification of the bubble method for the compliance minimization problems of plates and spherical shells. *Proc. 3rd World Congress of Structural and Multidisciplinary Optimization (WCSMO-3)* (held in Buffalo, NY)

Lin, C.Y.; Chao, L.-S. 2000: Automated image interpretation for integrated topology and shape optimization. *Struct. Multidisc. Optim.* **20**, 125–137

Mlejnek, H.P. 1992: Some aspects of the genesis of structures. *Struct. Optim.* **5**, 64–69

Osher, S.; Sethian, J.A. 1988: Front propagating with curvature-dependent speed: algorithms based on Hamilton–Jacobi formulations. *J. Comput. Phys.* **79**, 12–49

Osher, S.; Fedkiw, R. Level set methods: an overview and some recent results. *J. Comput. Phys.* **169**, 475–502

Peng, D.; Merriman, B.; Osher, S.; Zhao, H.-K.; Kang, M. 1999: A PED-based fast local level set method. *J. Comput. Phys.* **155**, 410–438

Reynolds, D.; McConnachie, J.P.; Bettess, W.; Christie, C.; J. Bull, W. 1999: Reverse Adaptivity – a new evolutionary tool for structural optimization. *Int. J. Numer. Methods Eng.* **45**, 529–552

Rozvany, G. 1989: *Structural Design via Optimality Criteria*. Dordrecht: Kluwer

Rozvany, G.; Zhou, M. 1991: The COC algorithm, Part II: topological, geometrical and generalized shape optimization. *Comput. Methods Appl. Mech. Eng.* **89**, 309–336

Rozvany, G.; Zhou, M.; Birker, T. 1992: Generalized shape optimization without homogenization. *Struct. Optim.* **4**, 250–252

Rozvany, G. 2001: Aims, scope, methods, history and unified terminology of computer aided topology optimization in structural mechanics. *Struct. Multidisc. Optim.* **21**, 90–108

Sapiro, G. 2001: *Geometric Partial Differential Equations and Image Analysis*. Cambridge: Cambridge University Press

Sethian, J.A.; Wiegmann, A. 2000: Structural boundary design via level set and immersed interface methods. *J. Comput. Phys.* **163**(2), 489–528

Sethian, J.A. 1999: *Level Set Methods and Fast Marching Methods: Evolving Interfaces in Computational Geometry, Fluid Mechanics, Computer Vision, and Materials Science*. Cambridge: Cambridge University Press

Shu, C.-W. 1988: Total-variation-diminishing time discretization. *SIAM J. Sci. Stat. Comput.* **9**, 1073–1084

Shu, C.-W.; Osher, S. 1988: Efficient implementation of essentially non-oscillatory shock capture schemes. *J. Comput. Phys.* **77**, 439–471

Sigmund, O. 2000: Topology optimization: A tool for the tailoring of structures and materials. *Philos. Trans.: Math. Phys. Eng. Sci.* **358**, 211–228

Sigmund, O. 2001: A 99 topology optimization code written in Matlab. *Struct. Multidisc. Optim.* **21**, 120–718

Sokolowski, J.; Zochowski, A. 1999: On the topological derivative in shape optimization. *SIAM J. Control Optim.* **37**(4), 1251–1272

Sokolowski, J.; Zolesio, J.P. 1992: *Introduction to Shape Optimization: Shape Sensitivity Analysis*. New York: Springer-Verlag

Suzuki, K.; Kikuchi, N. 1991: A homogenization method for shape and topology optimization. *Comput. Methods Appl. Mech. Eng.* **93**, 291–381

Wang, M.Y.; Wang, X.M.; Guo, D.M. 2003: A level set method for structural topology optimization. *Comput. Methods Appl. Mech. Eng.* **192**(1-2), 227–246

Wang, M.Y.; Wang, X.M. 2003: A multi-phase level set model for multi-material structural optimization. *Proc. 5th World Congress of Structural and Multidisciplinary Optimization (WCSMO5)* (held in Lido di Jesolo, Italy)

Xie, Y.M.; Steven, G.P. 1997: *Evolutionary Structural Optimization*. New York: Springer